ASSESSING AIRFLOW DISTRIBUTION IN VENTS OF A NATURALLY VENTILATED TEST FACILITY USING REFERENCE AIR VELOCITY MEASUREMENTS

G. De Vogeleer, P. Demeyer, P. Van Overbeke, J. G. Pieters

ABSTRACT. *Emission measurement in naturally ventilated buildings is a complex task because wind conditions can change quickly, inducing high spatial and temporal variations in the air velocity and pollutant concentration at the vent level. Simply taking the product of differential pollutant concentration and airflow rate may generate inaccurate results because the limited number of measurement locations usually fails to correctly reflect the velocity and concentration distributions in the vents. To assess the predictability of the airflow distribution in the vents of a naturally ventilated building, detailed measurements were conducted in the vents. Linear regression was applied to velocity measurements taken in the vents and at a 10 m mast (meteomast) located 20 m away. The detailed airflow measurements were used to validate statistical models. Results showed that the velocity distribution in the ridge vent could be modeled accurately and precisely for all wind directions (R^2 > 89%). Models for unidirectional airflows showed high predictability for the side vent (R^2 > 92%). Models for bidirectional airflows showed good predictability for the windward side when the air flowed in the same direction as the outside wind (R^2 > 88%) but showed less accurate results for the leeward side as well as for airflows moving in the opposite direction to the outside wind. For all models and wind directions, the most important input variable was the velocity component measured perpendicular to the vents at the meteomast. The importance of the velocity component measured parallel to the vents increased near the edges of the vent when the vent was on the windward side but did not reach the importance of the perpendicular component. The results confirmed the importance of using different models for unidirectional and bidirectional airflows to obtain accurate airflow assessments.*

Keywords. *Airflow rate distribution, Mock-up building, Natural ventilation, Ultrasonic anemometer.*

Ammonia emission and deposition in the environment contribute to eutrophication and acidification of soil and water. More than 90% of the ammonia emissions in Europe originate from animal husbandry (Eurostat, 2013). Assessing these emissions is important to determine the emission factors of animal houses and to evaluate the efficiency of mitigation techniques. One of the main suggested measurement methods involves calculating the emission as the product of differential pollutant concentration and airflow rate. However, especially for naturally ventilated buildings, measuring emissions is not straightforward in practice due to uncertainties that are largely unknown (Calvet et al., 2010; Samer et al., 2011). The uncertainties related to measuring emissions from these buildings are mostly a consequence of the high spatial and temporal variations in the velocity distribution in the vents due to constantly changing weather conditions (Ogink et al., 2013; Seifert et al., 2006), especially for large openings. Furthermore, large openings can act as inlets and outlets at the same time (called bidirectional flow) (Demmers et al., 2000; Etheridge, 2015; Özcan et al., 2009; Wu et al., 2012; Zhang et al., 2005). The direction of the airflow in the opening can change between different parts of the opening in a short time (Bruce, 1978).

When measuring the airflow rate with direct measurement methods, the number of measuring points in the vent is inversely proportional to the uncertainty of the method (Joo et al., 2014): the fewer the measurement points, the less information is collected about the airflow. The location of the measurement points also influences the information collected on the spatial distribution of airflow (Kiwan et al., 2012; Saha et al., 2013; Van Buggenhout et al., 2009). In most studies with direct measurement, sensors are equally spaced over the surface area of the vent (Calvet et al., 2013; Kiwan et al., 2012; López et al., 2011) or a sensor is traversed across the opening in time steps (Faggianelli et al., 2015; López et al., 2011; Van Overbeke et al., 2015). Measurement locations in vent openings are typically determined as a compromise based on the availability of sensors (Faggianelli et al., 2015) and costs. For monitoring design and cost efficiency, knowledge of the airflow distribution and direction in different vent openings under a wide range of wind conditions is important.

Despite this importance, research on the airflow distribu-

Submitted for review in May 2017 as manuscript number PAFS 12458; approved for publication by the Plant, Animal, & Facility Systems Community of ASABE in January 2018.

The authors are **Gerlinde De Vogeleer,** Research Engineer, **Peter Demeyer,** Research Engineer, and **Philippe Van Overbeke,** Research Engineer, Department of Agricultural Engineering, Institute for Agriculture, Fisheries, and Food (ILVO), Merelbeke, Belgium, and **Jan G. Pieters,** Professor, Faculty of Bioscience Engineering, Ghent University, Ghent, Belgium. **Corresponding author:** Gerlinde De Vogeleer, ILVO, Burg. Van Gansberghelaan 115, 9820 Merelbeke, Belgium; phone: 0032-9-2722547; e-mail: gerlinde.devogeleer@ilvo.vlaanderen.be.

  ISSN 2151-0032 https://doi.org/10.13031/trans.12458

tion in vent openings is scarce. Experiments have been performed on air velocity patterns in greenhouses (Kiwan et al., 2012; Faggianelli et al., 2015; Wang et al., 1999), commercial buildings (Nielsen, 2015), and dairy barns (Fiedler and Müller, 2011; Norton et al., 2009; Wu et al., 2012). Although many experiments have been done using velocity measurements in vents (De Vogeleer et al., 2016; Joo et al., 2014, 2015; Molina-Aiz et al., 2009; Wang et al., 2016), most of the measurement results were used to calculate the total airflow rate through the building, while the behavior of the velocity distributions in the vent openings remained unexplored.

However, some interesting research at the vent opening level has been performed concerning the behavior of inlet and outlet airflows, velocity distributions, and the steadiness or fluctuation of the airflow. Multiple studies have demonstrated that the inlet or outlet behavior of vent openings depends on the wind incidence angle (Boulard and Wang, 2002; López et al., 2011; Shilo et al., 2004; Teitel et al., 2008a). Choinière and Munroe (1994) and Teitel et al. (2005) introduced a "critical incidence angle" for which the airflow direction can change in a vent opening. Other studies (Li et al., 2000; Wang and Chen, 2012) focused on bidirectionality in vent openings due to the buoyancy effect (with a horizontal neutral plane). Choinière and Munroe (1994) and Teitel et al. (2008b) found that wind perpendicular to the opening plane provided the most uniform airflow patterns in vents and inside buildings. Kiwan et al. (2012) studied the effect of sensor placement in the vent opening. They stated that measuring the air velocity at different points in the opening to obtain representative data for the whole opening is more important than measuring a large number of openings located in similar positions.

Regarding the steadiness of the air velocity in vent openings, Kiwan et al. (2012) found that fluctuations of the velocity were dependent on the measurement location. Faggianelli et al. (2015) stated that when the airspeed profile is stable enough, i.e., correlating single measurements in the opening to a reference measurement for the opening, the number of sensors can be limited. However, the conditions are not always suitable for correlating single measurements to a reference measurement, as the fluctuations of the outside wind are random and unknown (Ji et al., 2011).

To obtain efficient sampling of the airflow rates or emissions from a building by measuring the airflow in the vents, research is needed to obtain an in-depth understanding of the velocity distribution in the vents and the influencing factors. One of the first steps toward understanding the velocity distribution is to measure it and link it to outside weather conditions.

The objective of this research was to assess the predictability of the airflow distribution across the vents of a naturally ventilated building. This was done using detailed sampling of the air velocities in the vents and statistical modeling of all incoming and outgoing airflow rates through the ridge and side vents of a test facility. The spatial and temporal distributions of unidirectional and bidirectional airflow rates were analyzed.

Materials and Methods

Test Facility, Instrumentation, and Experimental Setup

The measurements were conducted at a test facility in Merelbeke, Belgium (50° 58′ 38.56″ N, 3° 46′ 45.68″ E). The building represents a section of a typical Flemish pig barn. The building is in an open field with the nearest building at 50 m distance (fig. 1). Dimensions of the facility are 12.0 m × 5.3 m × 4.9 m (length × width × ridge height), yielding an internal volume of 251 m^3 (fig. 2). The ridge, with dimensions of 0.3 m × 4.0 m, has upright flanges of 0.3 m height and was placed in the middle of the length of

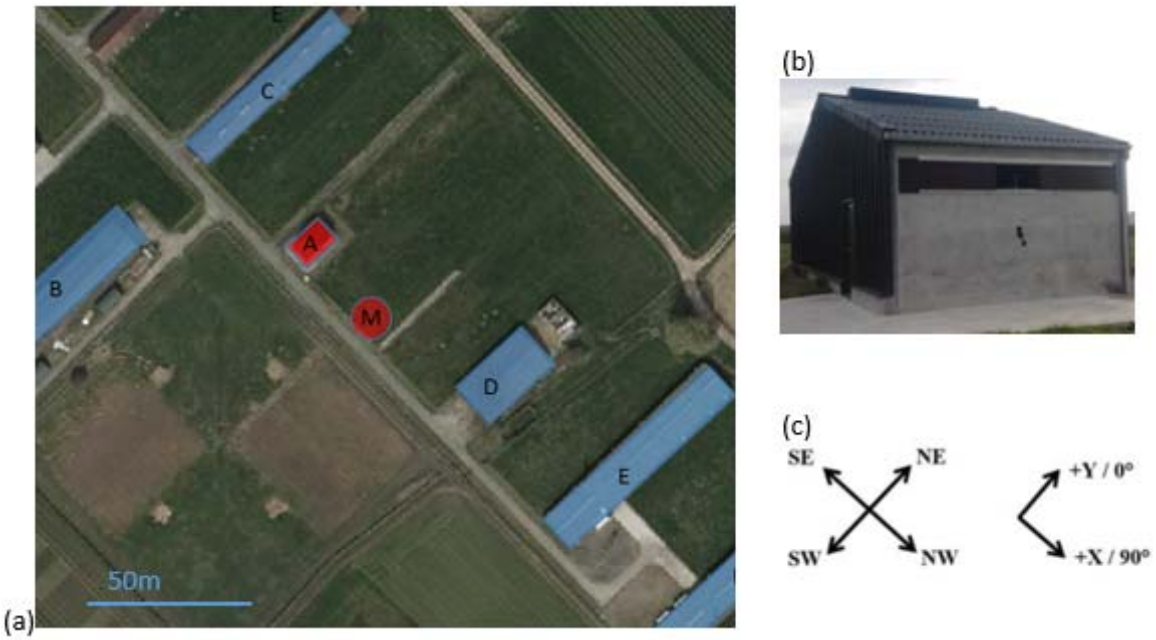

Figure 1. (a) Site of the test facility (building A is the test facility, buildings B, C, D, and E are at least 50 m from the test facility, and M is the meteomast), (b) photo of the test facility, and (c) compass directions and positioning of the tangential and normal vector components.

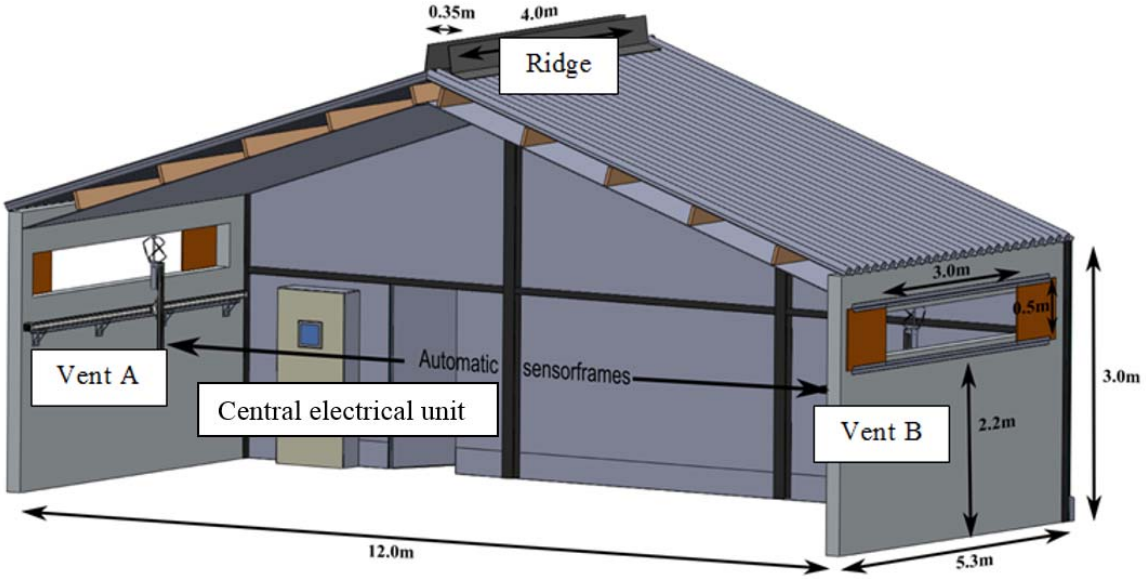

Figure 2. Cutaway of the test facility at the Flanders Research Institute for Agriculture, Fisheries, and Food (ILVO) in Merelbeke, Belgium.

the test facility, so the facility is symmetrical around the vertical plane through the ridge.

Two side vents (0.5 m × 4.5 m with a depth of 0.2 m) are located in opposite concrete walls. One side vent faces southwest (the main wind direction), and the opposite vent faces northeast. Only small obstacles to the airflow are present in the test facility. A central electrical unit (with wiring, datalogger, and related hardware) and a switch box for the electricity are mounted on the interior walls of the building. The test facility is assumed to be symmetrical, although the abovementioned small obstacles and a sealed door and gate are present. The surrounding buildings are located far enough way to allow unimpeded airflow around and through the test facility.

Because small and large airflow rates were of equal importance (models were built on the full range of wind speeds), measurement uncertainties caused by leakages had to be reduced as much as possible. The building was therefore pressurized by installing a fan in one side vent and sealing all large openings. The test facility was filled with smoke to visualize possible leaks, which were then sealed to the extent possible.

During the measurement experiments, all vent openings were equipped with ultrasonic anemometers. The ridge opening had eight fixed 2D ultrasonic anemometers (Thies, Göttingen, Germany). These were mounted as much as possible in the middle of the width and spaced equally along the length of the ridge opening on the longitudinal axis. Each side opening was equipped with a 3D ultrasonic anemometer (Thies, Göttingen, Germany) installed on an automatically controlled linear guiding system. This system allowed 2D movement of the sensor across the vent opening (Van Overbeke et al., 2015).

To measure the outside wind conditions, a 10 m high telescopic mast with a 2D ultrasonic anemometer (Thies, Göttingen, Germany), called the meteomast, was installed 20 m from the test facility. The 2D and 3D anemometers measured data at frequencies of 50 and 33 Hz, respectively. Results were stored as 1 s averages in a central logger (DT85M, DataTaker, Scoresby, Australia) via a serial (RS-422) interface.

Reference Airflow Measurements and Calculations

The airflow measurements were conducted using the method of Van Overbeke et al. (2014a, 2014b, 2015) based on direct measurements in the vent openings using ultrasonic anemometers. Each measurement location in each side vent was sampled for 10 s at 1 Hz with the automatic mobile sensor. For each measurement location, an average velocity was calculated to filter the instantaneous values. The air velocity measurements at the ridge were collected continuously with the fixed anemometers installed there.

For all measurement locations (ridge and side vents), a separate moving average velocity was calculated with the data obtained during the last ten measurement rounds (approx. 1.5 h). Measurement at all locations in a side vent (one round) took approximately 10 min. For each location, the mean air velocity was calculated for each round. The air velocity at each location was measured with the moving sensor during ten rounds (ten measurement intervals of 10 × 1 s). For the ridge vent, the air velocity at each location was measured with a fixed sensor during 480 × 1 s. The mean air velocity measurements resulted in a detailed analysis of the airflow through the vents of the test facility. These data can be used to evaluate the airflow distribution at building level, vent level, or in different parts of the openings.

Airflow at Measurement Locations

The grid of the measurement locations in the side openings was determined by the size of the sensor head. The sensor head had dimensions of approximately 0.25 m × 0.125 m, which was used as the surface area per measurement location. These dimensions resulted in a matrix of 4 rows and 12 columns within the opening (48 measurement locations). The ridge vent was equipped with eight fixed anemometers (one anemometer failed during measurements), giving a surface area of 0.35 m × 0.5 m per measurement location. The

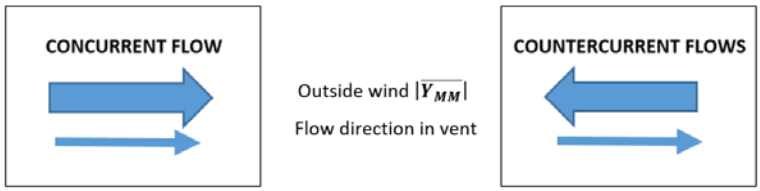

Figure 3. Flow direction of the outside wind ($|\overline{Y_{MM}}|$) and of the airflow in the vent for concurrent and countercurrent flows.

airflow magnitude (m s^{-1}) and direction were measured at each location. The airflow direction was defined as concurrent or countercurrent according to the direction of the outside wind (fig. 3).

Airflow at Partition Level

The vent openings were divided into partitions to facilitate modeling of the airflow distribution. For all openings (ridge and side vents), four partitions were used. The ridge opening had two measurement locations in each partition, and the side vents had 12 measurement locations (4 rows and 3 columns) in each partition (fig. 4). Because the side vents were wider than they were high, only horizontal partitions and no vertical partitions were used in these openings. Vertical partitions were not of interest because no extra heat was added; thus, isothermal conditions were assumed (a maximum of 1°C was measured between inlet and outlet airflows), and no stack effect was expected (De Vogeleer et al., 2016). Furthermore, due to the limited height of the vents and of the building, no effects of the boundary layer were expected.

Each partition in an opening represented a partial airflow rate; thus, the sum of all partial airflow rates resulted in the full airflow rate through the opening. These partial airflow rates were calculated using the velocities at each measurement location by summing the products of the surface area and the velocity measured of that location:

$$Q_{part} = \sum_{j=1}^{N} \left(\left| \overline{Y_{ms}} \right|_j \times A_j \times 3600 \right) \quad (1)$$

where

Q_{part} = partial airflow rate (m^3 h^{-1})
ms = measurement surface
j = measurement location
$|\overline{Y_{ms}}|$ = mean normal velocity component at location *j* (m s^{-1})
A = surface area (m^2)
N = total number of measurement locations within a partition (i.e., 12 for a side vent partition, and two for a ridge vent partition).

The measurement surfaces were measured horizontally, starting at the lowest row. The airflows were assigned a symbol indicating their direction relative to the building. A plus sign indicated air flowing into the test facility (inflow; +*Q*), while a minus sign indicated air flowing out of the building (outflow; –*Q*). For each partition, the incoming and outgoing airflow rates were calculated by taking the sum of the positive or negative airflow rates, respectively, for the measurement locations of that partition.

Airflow at Building Level

Using the data for all measurement locations, the inflow and outflow rates for an opening or for the entire test facility could be calculated. The airflow rates for the building were calculated using a equation similar to that used for the partitions:

$$Q_{tot} = \sum_{k=1}^{N} \left(\left| \overline{Y_{ms}} \right|_k \times A_k \times 3600 \right) \quad (2)$$

where

Q_{tot} = mean airflow rate through the building over approximately 1.5 h (m^3 h^{-1})
$|\overline{Y_{ms}}|_k$ = mean normal velocity component (m s^{-1})
A_k = surface area of measurement location *k* (m^2)
N = total number of surface areas within an opening (i.e., 48 for a side vent, and eight for a ridge vent).

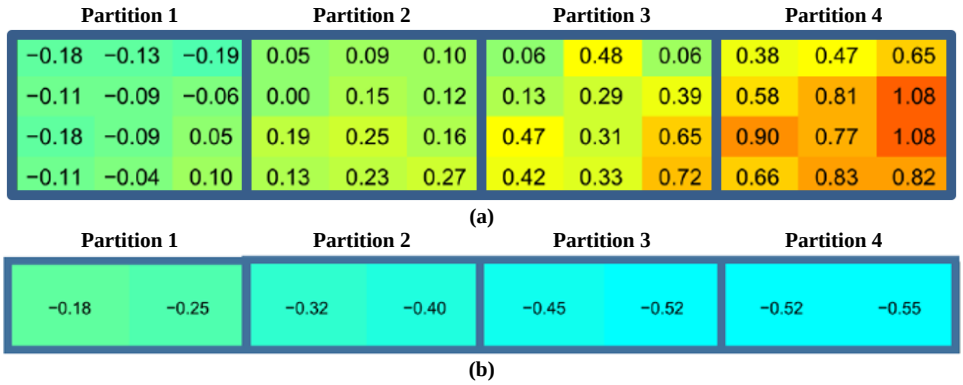

Figure 4. Measurement locations in four partitions for the (a) side vents and (b) ridge vent. Values represent mean airflow velocities (m s^{-1}) over 1.5 h. Colors indicate wind magnitude and direction: light red to dark red represents small to large magnitudes for wind sector 1, and light blue to dark blue represents small to large magnitudes for wind sector 2.

The total inflow and outflow were calculated together with their respective surface areas. Measurements were taken continually from December 2014 to March 2015.

Data Collection

Because the test facility was symmetrical around the vertical plane through the ridge, only one side opening (facing southwest) and the ridge opening were examined for airflow distribution. This study used airflow rates at the partition level to build the airflow models. The airflow data at the partition level were divided into different groups. First, the dataset was split depending on whether the approaching airflow directly entered the vent opening or first passed through the inside of the building. To indicate the wind direction relative to the opening, all measurements were assigned a perpendicular component: $+Y$ for winds from 90° to 270° (wind sector 1) and $-Y$ for winds from 270° to 360° and from 0° to 90° (wind sector 2) (fig. 5).

Second, we defined the airflow at the partition level as unidirectional if the opening acted exclusively as an inlet or an outlet or as bidirectional if the opening acted simultaneously as an inlet and an outlet. A partition was considered bidirectional when at least one velocity measurement in that partition had a different sign, i.e., plus or minus, indicating a countercurrent (fig. 3) from the other measurements. If the airflow was determined to be bidirectional, the inflow and outflow rates for the partition were calculated separately and were defined afterward as concurrent if the airflow had the same direction as the wind at the meteomast or countercurrent if the airflow had the opposite direction of the wind at the meteomast (figs. 3 and 5).

Model Development

Multiple linear regression (eq. 3) was used to model the partial airflow rates at the partition level, as used by De Vogeleer et al. (2016). These statistical models gave information about the velocity distribution in the openings and are called distribution models in the Results and Discussion section.

The $\left|\overline{X_{MM}}\right|$ and $\left|\overline{Y_{MM}}\right|$ velocity components measured at the meteomast were used as independent variables, with the airflow rate at the partition level as the dependent variable. All statistical modeling was performed in Matlab (ver. 8.6). Coefficients a, b, and c of the multiple regression model and regression analysis were determined by applying curve-fitting methods. The normality of the error distribution was checked with Q-Q plots (residual plots), and 95% confidence intervals were calculated using the Matlab confint code. All modeled partial airflow rates were compared to all measured partial airflow rates using single linear regression (eq. 4):

$$Q_{modelled} = \boldsymbol{a} \times \left|\overline{X_{MM}}\right| + \boldsymbol{b} \times \left|\overline{Y_{MM}}\right| + \boldsymbol{c} \tag{3}$$

$$Q_{reference} = \boldsymbol{p} \times Q_{modelled} + \boldsymbol{d} \tag{4}$$

where

a, b = coefficients (m^2)
c, d = coefficients ($m^3\ h^{-1}$)
p = constant (dimensionless)
$Q_{reference}$ = measured airflow rates at partition level ($m^3\ h^{-1}$)
$Q_{modeled}$ = modeled airflow rates at partition level ($m^3\ h^{-1}$).

The agreement between the modeled and measured airflow rates was assessed using two different methods: regression, as described above, and Bland-Altman analysis (Bland and Altman, 2010). The coefficient of determination, slope, and intercept of the single linear regression were used to indicate how well the model fitted the data. The Bland-Altman analysis was used as a residual plot to indicate how the absolute difference between the modeled and measured results was related to the average of the modeled and measured results. This agreement between the modeled and measured results was analyzed with the slope (β_0) and intercept (β_1) (eq. 5):

$$\left(Q_{modelled} - Q_{reference}\right) = \boldsymbol{\beta}_0 \times \frac{Q_{modelled} + Q_{reference}}{2} + \boldsymbol{\beta}_1 \tag{5}$$

where β_0 is the slope (dimensionless), and β_1 is the intercept ($m^3\ h^{-1}$). An ideal model results in coefficients close to zero.

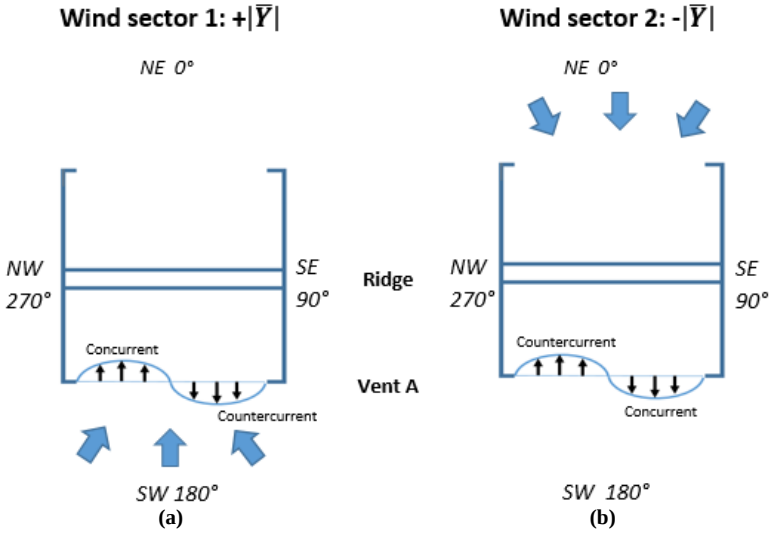

Figure 5. Wind direction and definition of concurrent and countercurrent flows for (a) wind sector 1 and (b) wind sector 2.

The analysis results were used to describe the statistical models in terms of accuracy and precision. Accuracy is associated with systematic errors, as it describes how close a modeled value is to the actual value. In this study, accuracy is defined by low residuals between the modeled and measured airflow rates (using Bland-Altman analysis). Precision is associated with random errors, as it describes how close the measured values of the same airflow rate are to each other (repeatability) (JCGM, 2008).

RESULTS AND DISCUSSION

EXPERIMENTAL DATA

The wind conditions during the measurements were representative of typical weather in Flanders. The typical wind speed was 2 to 3 m s^{-1} (fig. 6a). More data points (5998 measured airflow rates of 1.5 h each) were measured for wind sector 1 (fig. 6b) than for wind sector 2 (1172 airflow rates). Wind speeds were up to 12 m s^{-1}, with the highest peaks recorded for wind sector 1.

The absolute inflow and outflow rates through the side and ridge vents, plotted in figures 7c and 7d, show that the ridge acted mainly as an outlet, independent of the wind direction (positive or negative $\left|\overline{Y_{MM}}\right|$). For approximately 1% of the measured airflow rates at vent level, air also entered the test facility through the ridge. The side vent acted as an inlet and/or an outlet depending on the wind direction. The ratio of the incoming and outgoing airflows was not necessarily equal to the ratio of the surface areas of the incoming and outgoing airflows (fig. 7b) because of spatial variations in the velocity distribution in the openings. Although the countercurrent airflow rates through the side vent were very small, the respective relative surface areas were larger than expected based on the partition area, which could be of great importance for emission and/or airflow rate measurements. For example, 75% of the airflow could flow through 25% of the opening area.

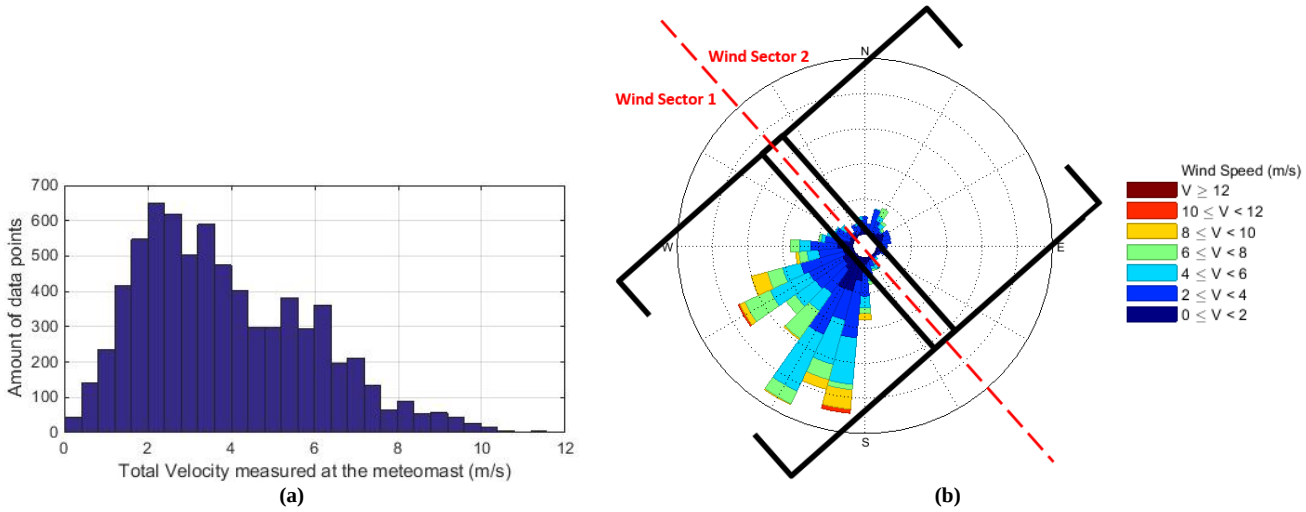

Figure 6. (a) Distribution of mean air velocity during measurements and (b) outline of test facility projected onto a compass showing wind speed and direction. Concentric circles on the compass indicate frequency of occurrence in increments of 3%.

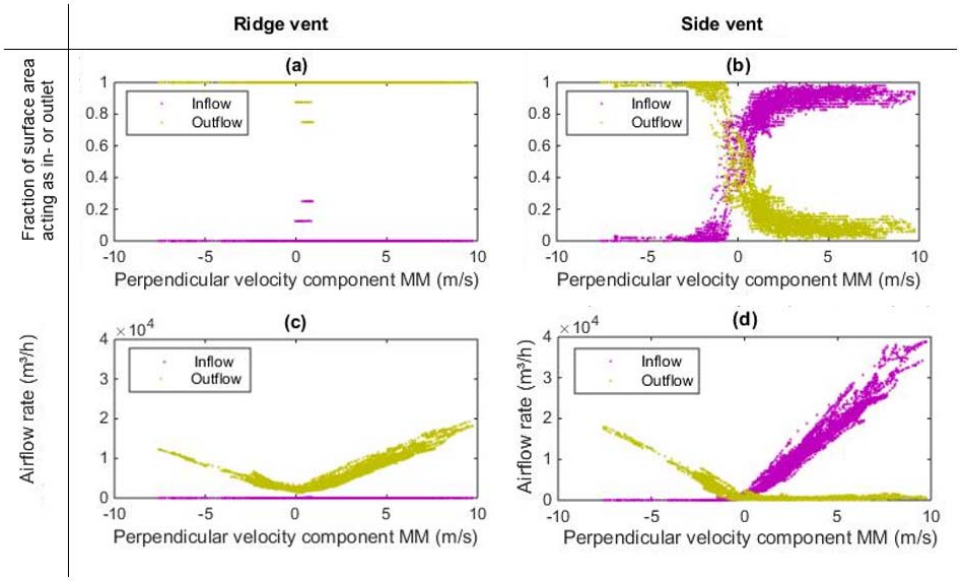

Figure 7. Fraction of vent surface area acting as inlet or outlet for the (a) ridge vent and (b) side vent and airflow rate through the (c) ridge vent and (d) side vent as a function of the perpendicular wind velocity component at the meteomast (*MM*) (m^3 s^{-1}).

The maximum outgoing airflow rates for the ridge were 19,254 and 12,253 $m^3 h^{-1}$ for wind from sectors 1 and 2, respectively. The maximum inflow and outflow rates for the side vent were 38,975 and 2224 $m^3 h^{-1}$, respectively, for wind from sector 1 and 17,987 and 1755 $m^3 h^{-1}$, respectively, with wind from sector 2. The airflow rates for wind sector 1 were generally higher than those for wind sector 2, as expected based on the measured wind conditions during the experiment.

Distribution Models for Ridge Vent

The experiments in the test facility showed that the ridge vent almost always acted as a unidirectional outlet. For both wind sectors 1 and 2, some airflow rates acted bidirectionally (0.01% and 0.001%, respectively), but these were so few and so small that they were omitted from the modeling. The coefficients for each wind sector, shown in figure 8, can be applied to a multiple linear regression model to assess the airflow rate through each partition of the ridge vent. Due to the large number of observations, the error bars of the coefficients are so small that they are almost undetectable. This was confirmed by a slope of nearly zero and a low intercept (compared to the maximum airflow rate) for the Bland-Altman analysis (table 1). For all cases, regression analysis gave slopes of one and intercepts that were not significantly different from zero. This means that the models for the ridge vent were very accurate and precise (high R^2 values; table 1).

Because the test facility was nearly symmetrical, it was expected that the coefficients would be comparable for both wind sectors. Differences in coefficients *b* and *c* between the wind sectors could result from dissimilarities in the landscape for the two wind sectors or because the data set for wind sector 2 did not have the same wide range of velocities as sector 1. Parallel wind components seemed to have only a small effect on the airflow rate through the partitions of the ridge vent (small *a* coefficient). The values of coefficient *b* for input variable $\left|\overline{Y_{MM}}\right|$ were highest in number for both wind sectors, which made $\left|\overline{Y_{MM}}\right|$ the most important input variable to assess the airflow rate. For wind sector 2, the intercept *c* lay in the same range as coefficient *b*; however, when the perpendicular velocity increased, the intercept decreased in importance.

Distribution Models for Side Vent

Unidirectional Flows

The model coefficients for unidirectional flows in the different partitions of the side vent are shown in figure 9. The error bars of the coefficients are so small that they are almost undetectable. Overall, $\left|\overline{Y_{MM}}\right|$ is the most important variable, but coefficient *b* of $\left|\overline{Y_{MM}}\right|$ is larger for wind sector 1 than for wind sector 2. This is because the side vent is the main inlet for wind sector 1. For wind sector 2, the side vent is a shared outlet with the ridge vent. For winds coming from sector 2, the ridge and side vents had similar *b* coefficients, i.e., approximately 400 and 600 m^2. This implies that they were both important outlets.

The $\left|\overline{X_{MM}}\right|$ velocity component had little influence in general. For wind sector 2, this influence, compared to the other components, was stable over all partitions. Because the side vent was on the leeward side for wind sector 1, a uniform velocity pattern was expected, as seen in figure 9. For the outermost partitions with wind sector 1, when the side vent was on the windward side, the influence of $\left|\overline{X_{MM}}\right|$ greatly increased.

The intercept *c* was of the same magnitude for both wind sectors (100 to 150 $m^3 h^{-1}$) and became negligible for higher wind velocities, especially for higher values of $\left|\overline{Y_{MM}}\right|$.

When the opening was on the windward side (wind sector 1), coefficients *b* and *c* remained stable across all partitions, and only *a* was affected by the side vent.

Similar to the results for the ridge vent, the slope and intercept of the airflow models for unidirectional flows through the side vent were close to one and nearly zero, respectively. The coefficients of determination (table 2)

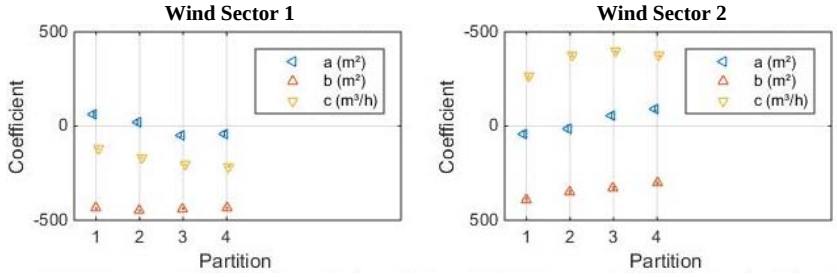

Figure 8. Coefficients of multiple linear regression for unidirectional flows in the ridge vent for (a) wind sector 1 and (b) wind sector 2. Error bars are 95% confidence boundaries.

Table 1. Analysis results per wind sector for each partition in the ridge vent: regression analysis (R^2), Bland-Altman analysis (β_0, β_1), maximum airflow rate through the partition ($m^3 h^{-1}$), and number of data points (*n*).

	Wind Sector 1					Wind Sector 2				
Partition	R^2	β_0	β_1	Max.	*n*	R^2	β_0	β_1	Max.	*n*
1	0.95	-0.03	-43	-5001	5961	0.92	-0.04	-47	-3245	1171
2	0.95	-0.03	-44	-4970	5998	0.89	-0.06	-63	-3122	1172
3	0.94	-0.03	-53	-4760	5998	0.92	-0.04	-45	-3052	1172
4	0.93	-0.03	-60	-4737	5998	0.94	-0.03	-32	-2835	1172

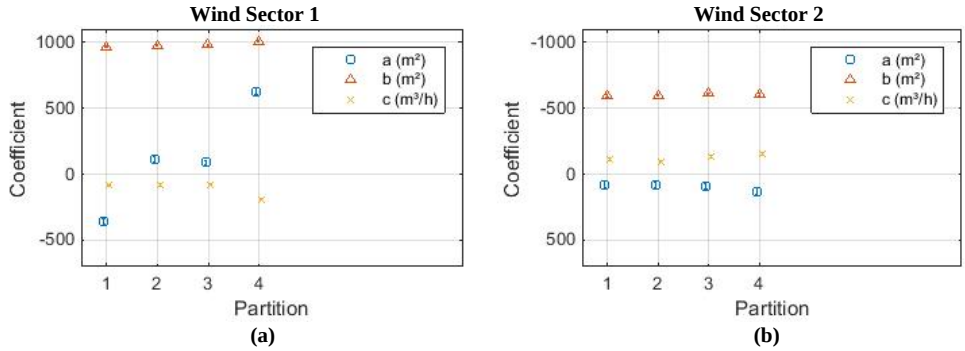

Figure 9. Coefficients of multiple linear regression for unidirectional flows in the side vent for (a) wind sector 1 and (b) wind sector 2. Error bars are 95% confidence boundaries.

Table 2. Analysis results per wind sector for unidirectional flows in each partition of the side vent: regression analysis (R^2), Bland-Altman analysis (β_0, β_1), the maximum of minimum airflow rate through the partition ($m^3\ h^{-1}$) and number of data points (*n*).

	Wind Sector 1					Wind Sector 2				
Partition	R^2	β_0	β_1	Max.	*n*	R^2	β_0	β_1	Min.	*n*
1	0.98	-0.01	43	11443	5553	0.92	-0.04	-48	-4733	1040
2	0.96	-0.02	69	10055	5863	0.96	-0.02	-27	-4335	1028
3	0.97	-0.02	51	9972	5922	0.96	-0.02	-24	-4505	1023
4	0.95	-0.03	86	12326	5274	0.95	-0.03	-34	-4583	1014

showed that, for both wind sectors, the variance in the airflow rates for unidirectional flows through the partitions could be almost fully explained with the $\left|\overline{X_{MM}}\right|$ and $\left|\overline{Y_{MM}}\right|$ input variables. The Bland-Altman coefficients showed that the results of the models followed the same trend as the reference airflow rates. These results showed good agreement between the modeled and measured airflow rates. It was possible to achieve an accurate and precise model to predict the airflow distribution in the side vent with the $\left|\overline{X_{MM}}\right|$ and $\left|\overline{Y_{MM}}\right|$ input variables measured at the meteomast.

Bidirectional Flows

The data for bidirectional flows were divided for the two wind sectors and based on the direction of the airflow compared to the outside wind (concurrent or countercurrent). The model coefficients for the airflow rates in the side vent with bidirectional flows are plotted in four graphs (fig. 10) for concurrent or countercurrent flows and wind sectors 1 and 2. The regression results for the modeled and measured airflow rates for all bidirectional flows gave promising results, with a slope of one and an intercept of nearly zero. This indicated that the models for all partitions and wind sectors for bidirectional flows are very accurate. The precision of

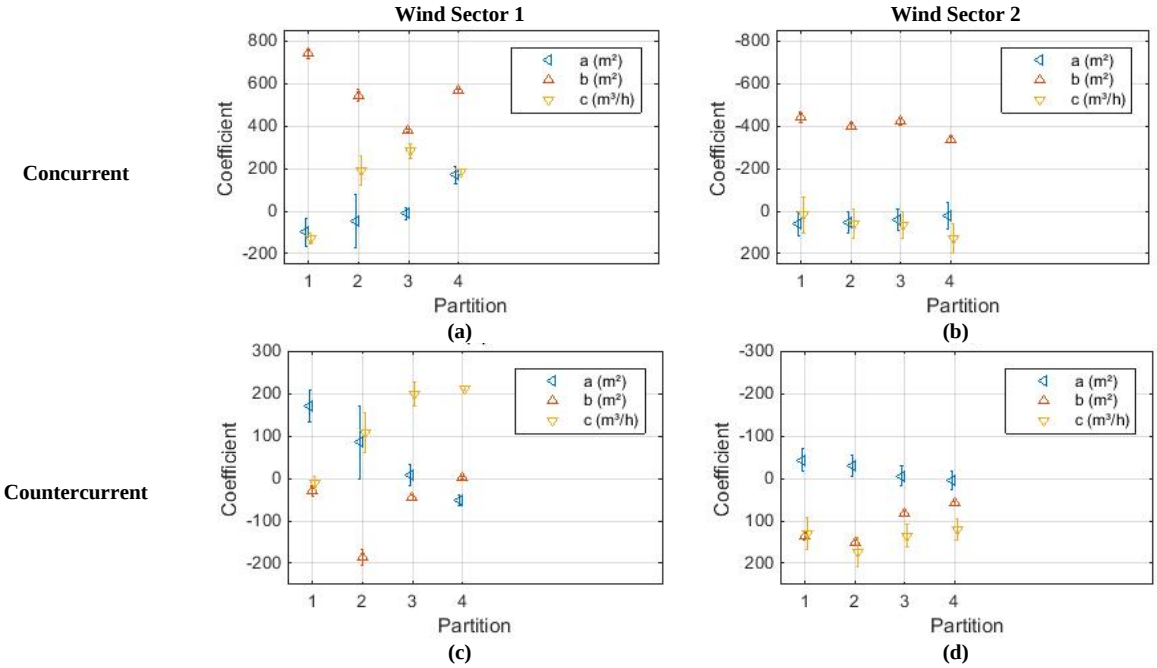

Figure 10. Coefficients of multiple linear regression for bidirectional flows in the side vent for (a) concurrent airflow for wind sector 1, (b) concurrent airflow for wind sector 2, (c) countercurrent airflow for wind sector 1, and (d) countercurrent airflow for wind sector 2. Error bars are 95% confidence boundaries.

the models can be determined by examining the results of the variance and the residual plots of the Bland-Altman analysis (tables 3 and 4).

The graphs for wind sector 2 show more stable coefficients and smaller error bars than for wind sector 1. This could be a result of the airflow for wind sector 2 first passing through the building before exiting through the side vent. The results for wind sector 1 varied considerably among partitions for both concurrent and countercurrent flows. This could have resulted from the direct influence of the wind on the measurements, as the air did not flow through the building first. This direct wind effect is also why wind sector 1 contained more bidirectional flow rate measurements for the outermost partitions, e.g., 724 measurements (12%) for partition 4 and 76 measurements for partition 3 (1.2%), while the number of measurements for wind sector 2 was relatively steady for all partitions (approx. 11% of all airflow rates for wind sector 2). Although wind sector 2 has the steadiest coefficients of the models, with smaller error bars, the R^2 values are overall lower and the residuals (lower β_0 and β_1) are relatively larger for all partitions and for both concurrent and countercurrent flows. Similar to the results for unidirectional flows, the $\left|\overline{X_{MM}}\right|$ velocity component had most influence on the outermost partitions with wind sector 1 and less influence on the inner partitions with wind sector 1 and on all partitions with wind sector 2.

Overall, coefficient *b* for the $\left|\overline{Y_{MM}}\right|$ input variable remained the largest component by weight. However, compared to the models for unidirectional flows, coefficient *a* for the $\left|\overline{X_{MM}}\right|$ input variable increased in importance with a higher value.

Comparison of the coefficients for unidirectional and bidirectional concurrent flows for wind sectors 1 and 2 (countercurrent flows are not presented for unidirectional flows) shows the importance of building separate models for airflow rates with unidirectional and bidirectional flows. This concurs with the findings of Calvet et al. (2013), Etheridge et al. (2012), and De Vogeleer et al. (2016). Both wind sectors gave lower values of the coefficients for concurrent flows (e.g., figs. 8 and 10).

Countercurrent flows produced models with a higher variance than concurrent flows. In addition, the Bland-Altman analysis revealed larger deviations between the modeled and measured results for countercurrent flows compared to concurrent flows. Possibly other parameters should also be considered.

The coefficients in figure 10 show that concurrent flows produced larger airflow rates than countercurrent flows. Figure 11 shows an example of all bidirectional flows, both concurrent and countercurrent, for wind sectors 1 and 2. The countercurrent flows for wind sector 2 are more scattered, which explains the low R^2 values.

General Discussion

The experiments in this study were conducted without internal obstructions inside the test facility and without other buildings in the immediate vicinity. Although these conditions were not entirely realistic for livestock buildings, the experiments were of great value because they involved detailed measurements in the vent openings of a full-scale test facility under outside wind conditions. These relatively simple circumstances provided an opportunity to make a detailed study of modeling partial airflow rates while giving weight to the known measurement factors.

The partial airflow rates in the ridge vent were modeled accurately and precisely for both wind sectors. All airflow rates of the partitions in the side vent for unidirectional flows were modeled accurately and precisely for both wind sectors. However, for bidirectional flows, only data for concurrent flows (approx. 90% of the data) gave good results. The models for countercurrent flows were accurate (i.e., a slope of one and an intercept of nearly zero when comparing modeled and measured results) but not very precise (low R^2 value). A possible explanation could be that the number of measurements was quite limited and that the airflow rates were relatively low and therefore more sensitive to unsteady wind conditions. An extra input variable could give better results, e.g., a local measurement within the partition. For this experiment, the bidirectional flows were limited in number compared to the total number of airflow measurements. However, in naturally ventilated buildings, such as dairy barns, bidirectional flows can occur more frequently due to the very large vents (Calvet et al., 2013; De Vogeleer et al., 2016; Etheridge, 2015).

These findings are also important in relation to measurements of NH_3 or CO_2 emissions, considering the effect of the airflow distribution on local concentration measurements in

Table 3. Analysis results per wind sector for bidirectional concurrent flows in each partition of the side vent: regression analysis (R^2), Bland-Altman analysis (β_0, β_1), maximum of minimum airflow rate through the partition ($m^3\ h^{-1}$), and number of data points (*n*).

	Wind Sector 1					Wind Sector 2				
Partition	R^2	β_0	β_1	Max.	*n*	R^2	β_0	β_1	Max.	*n*
1	0.88	-0.07	41	3668	445	0.53	-0.37	117	870	132
2	0.79	-0.13	45	1628	135	0.47	-0.44	139	824	144
3	0.90	-0.05	29	1053	76	0.56	-0.32	110	1294	149
4	0.89	-0.06	75	3983	724	0.38	-0.58	229	1029	158

Table 4. Analysis results per wind sector for bidirectional countercurrent flows in each partition of the side vent: regression analysis (R^2), Bland-Altman analysis (β_0, β_1), maximum of minimum airflow rate through the partition ($m^3\ h^{-1}$), and number of data points (*n*).

	Wind Sector 1					Wind Sector 2				
Partition	R^2	β_0	β_1	Max.	*n*	R^2	β_0	β_1	Max.	*n*
1	0.62	-0.27	114	1283	445	0.35	-0.64	37	506	132
2	0.71	-0.18	53	634	135	0.39	-0.56	46	405	144
3	0.29	-0.76	126	330	76	0.19	-1.02	80	476	149
4	0.67	-0.22	77	730	724	0.19	-1.02	69	456	158

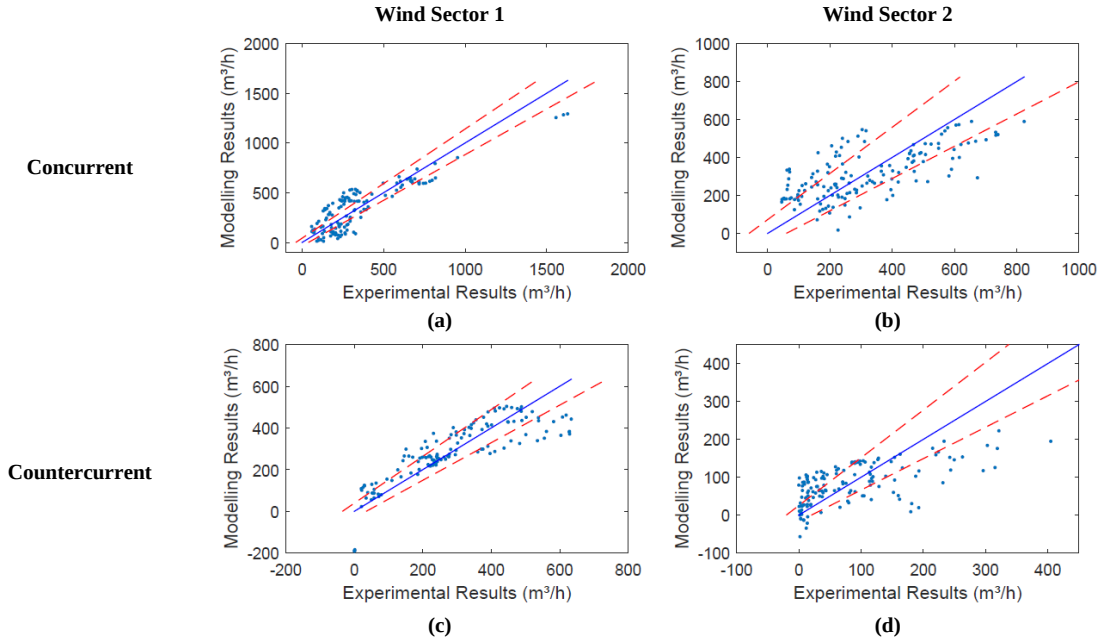

Figure 11. Examples of modeled airflow rates through partition 2 of the side vent for (a) concurrent airflow for wind sector 1, (b) concurrent airflow for wind sector 2, (c) countercurrent airflow for wind sector 1, and (d) countercurrent airflow for wind sector 2. Solid blue line is model line, and dashed red lines are 95% confidence intervals.

the vents. Information concerning airflow distribution in the vents is essential for an efficient concentration measurement campaign. Because the airflow rate per surface area is not equal for all locations in the vent opening, large airflows can pass through a small part of the opening. The information in this article can be used to choose the number and position of measurement locations.

The vent configuration (i.e., location, size, and presence or absence of windbreak nets) influences the ventilation rate and the distribution of air flowing through the building. Therefore, ventilation should always be considered at the building level instead of at the vent level. Due to disturbances in the surroundings (Jiang and Chen, 2002) (e.g., vent configuration, animal density, pen equipment, etc.), calibration is essential for any model to obtain accurate airflow rates.

Because the models for concurrent airflows were precise and accurate, it is expected that measurement campaigns can focus more on diverse measurement conditions, e.g., measuring under as many wind conditions as possible, and less on measurement repetitions.

The strength of a model depends on the quality of the measurements. Models combined with an additional variable in the vent opening could be especially useful when measuring in buildings with large vents, such as dairy barns, where bidirectional flows can occur more frequently or at higher airflow rates. Further research should focus on buildings with large vents to validate the findings of this study. Undoubtedly, the major challenge in successfully applying the proposed models is determining the model parameters for real-life conditions, based on measurements using reference techniques.

CONCLUSIONS

To analyze the airflow rate distribution and predictability in a naturally ventilated test facility, detailed measurements were performed in the vent openings. Multiple linear regression was applied to the measured data using air velocity measurements from a meteomast (10 m high) (De Vogeleer et al., 2016). The models were validated using detailed airflow measurements for the side and ridge openings that were obtained under different wind conditions. The airflow measurements were performed using the method of Van Overbeke et al. (2015). Models were built for different wind direction sectors and for the character of the flow at vent level, i.e., unidirectional or bidirectional. When the flow was bidirectional, concurrent flows (airflow in the same direction as the outside wind) and countercurrent flows (airflow in the opposite direction of the outside wind) were modeled. The velocity components from the meteomast data, $\left|\overline{X_{MM}}\right|$ and $\left|\overline{Y_{MM}}\right|$, were used as input variables in a linear regression model to calculate the airflow rates.

The airflow rates through all partitions of the ridge vent could be modeled accurately and precisely for both wind sectors (R^2 > 89%). The coefficients for all partitions of the ridge vent were comparable, and the coefficient for the $\left|\overline{Y_{MM}}\right|$ velocity component was the most important input variable for the ridge vent. The ridge vent behaved mostly as an outlet independent of the wind direction.

The airflow rates for the side vent behaved differently depending on the wind direction. The models showed that the predictability for the side vent was high for unidirectional flows (R^2 > 92%). Models for bidirectional flows showed good results at the windward side regardless of the wind direction (R^2 > 88%) but lower results at the leeward side. The

models for countercurrent flows showed larger deviations than those for concurrent flows. Possibly an extra input variable is needed for these types of models to improve their precision.

In general, it could be concluded that predictability of the airflow distribution in the vents of the test facility was feasible using measured airflow data from a nearby meteomast.

ACKNOWLEDGEMENTS

The authors are grateful for financial support from the Flanders Research Institute for Agriculture, Fisheries, and Food (ILVO) and the Agency for Innovation by Science and Technology (IWT) of the Flemish government (this study was partly conducted during Agricultural Research Project IWT090946). The authors thank the technicians at ILVO for their advice and support.

REFERENCES

Bland, J. M., & Altman, D. G. (2010). Statistical methods for assessing agreement between two methods of clinical measurement. *Intl. J. Nursing Studies, 47*(8), 931-936. https://doi.org/10.1016/j.ijnurstu.2009.10.001

Boulard, T., & Wang, S. (2002). Experimental and numerical studies on the heterogeneity of crop transpiration in a plastic tunnel. *Comput. Electron. Agric., 34*(1), 173-190. https://doi.org/10.1016/S0168-1699(01)00186-7

Bruce, J. M. (1978). Natural convection through openings and its application to cattle building ventilation. *J. Agric. Eng. Res., 23*(2), 151-167. https://doi.org/10.1016/0021-8634(78)90046-X

Calvet, S., Cambra-López, M., Blanes-Vidal, V., Estelles, F., & Torres, A. G. (2010). Ventilation rates in mechanically ventilated commercial poultry buildings in southern Europe: Measurement system development and uncertainty analysis. *Biosyst. Eng., 106*(4), 423-432. https://doi.org/10.1016/j.biosystemseng.2010.05.006

Calvet, S., Gates, R. S., Zhang, G., Estelles, F., Ogink, N. W., Pedersen, S., & Berckmans, D. (2013). Measuring gas emissions from livestock buildings: A review on uncertainty analysis and error sources. *Biosyst. Eng., 116*(3), 221-231. https://doi.org/10.1016/j.biosystemseng.2012.11.004

Choinière, Y., & Munroe, J. A. (1994). A wind tunnel study of wind direction effects on airflow patterns in naturally ventilated swine buildings. *Canadian Agric. Eng., 36*(2), 93-102.

De Vogeleer, G., Van Overbeke, P., Brusselman, E., Mendes, L. B., Pieters, J. G., & Demeyer, P. (2016). Assessing airflow rates of a naturally ventilated test facility using a fast and simple algorithm supported by local air velocity measurements. *Build. Environ., 104*, 198-207. https://doi.org/10.1016/j.buildenv.2016.05.006

Demmers, T. G., Burgess, L. R., Phillips, V. R., Clark, J. A., & Wathes, C. M. (2000). Assessment of techniques for measuring the ventilation rate, using an experimental building section. *J. Agric. Eng. Res., 76*(1), 71-81. https://doi.org/10.1006/jaer.2000.0532

Etheridge, D. (2012). *Natural ventilation of buildings.* Hoboken, NJ: John Wiley & Sons.

Etheridge, D. (2015). A perspective on fifty years of natural ventilation research. *Build. Environ., 91*, 51-60. https://doi.org/10.1016/j.buildenv.2015.02.033

Eurostat. (2013). Agriculture - Ammonia emission statistics. Luxembourg: Eurostat. Retrieved from http://ec.europa.eu/eurostat/statistics-explained/index.php/Agriculture_-_ammonia_emission_statistics

Faggianelli, G. A., Brun, A., Wurtz, E., & Muselli, M. (2015). Assessment of different airflow modeling approaches on a naturally ventilated Mediterranean building. *Energy Build., 107*, 345-354. https://doi.org/10.1016/j.enbuild.2015.08.038

Fiedler, A. M., & Müller, H. J. (2011). Emissions of ammonia and methane from a livestock building natural cross-ventilation. *Meteorol. Zeitschrift., 20*(1), 59-65. https://doi.org/10.1127/0941-2948/2011/0490

JCGM. (2008). International vocabulary of metrology: Basic and general concepts and associated terms (VIM). Geneva, Switzerland: ISO, Joint Committee for Guides in Metrology. Retrieved from https://www.bipm.org/utils/common/documents/jcgm/JCGM_200_2008.pdf

Ji, L., Tan, H., Kato, S., Bu, Z., & Takahashi, T. (2011). Wind tunnel investigation on influence of fluctuating wind direction on cross natural ventilation. *Build. Environ., 46*(12), 2490-2499. https://doi.org/10.1016/j.buildenv.2011.06.006

Jiang, Y., & Chen, Q. (2002). Effect of fluctuating wind direction on cross natural ventilation in buildings from large eddy simulation. *Build. Environ., 37*(4), 379-386.

Joo, H. S., Ndegwa, P. M., Heber, A. J., Bogan, B. W., Ni, J. Q., Cortus, E. L., & Ramirez-Dorronsoro, J. C. (2014). A direct method of measuring gaseous emissions from naturally ventilated dairy barns. *Atmos. Environ., 86*, 176-186. https://doi.org/10.1016/j.atmosenv.2013.12.030

Joo, H. S., Ndegwa, P. M., Heber, A. J., Ni, J. Q., Bogan, B. W., Ramirez-Dorronsoro, J. C., & Cortus, E. (2015). Greenhouse gas emissions from naturally ventilated freestall dairy barns. *Atmos. Environ., 102*, 384-392. https://doi.org/10.1016/j.atmosenv.2014.11.067

Kiwan, A. K., Berg, W., Brunsch, R., Özcan, S., Muller, H.-J., Glaser, M., ... Berckmans, D. (2012). Tracer gas technique, air velocity measurement, and natural ventilation method for estimating ventilation rates through naturally ventilated barns. *Agric. Eng. Intl.: CIGR J., 14*(4), 22-36.

Li, Y., Delsante, A., & Symons, J. (2000). Prediction of natural ventilation in buildings with large openings. *Build. Environ., 35*(3), 191-206. https://doi.org/10.1016/S0360-1323(99)00011-6

López, A., Valera, D. L., & Molina-Aiz, F. (2011). Sonic anemometry to measure natural ventilation in greenhouses. *Sensors, 11*(10), 9820-9838. Retrieved from http://www.mdpi.com/1424-8220/11/10/9820

Molina-Aiz, F. D., Valera, D. L., Pena, A. A., Gil, J. A., & López, A. (2009). A study of natural ventilation in an Almeria-type greenhouse with insect screens by means of tri-sonic anemometry. *Biosyst. Eng., 104*(2), 224-242. https://doi.org/10.1016/j.biosystemseng.2009.06.013

Nielsen, P. V. (2015). Fifty years of CFD for room air distribution. *Build. Environ., 91*, 78-90. https://doi.org/10.1016/j.buildenv.2015.02.035

Norton, T., Grant, J., Fallon, R., & Sun, D.-W. (2009). Assessing the ventilation effectiveness of naturally ventilated livestock buildings under wind-dominated conditions using computational fluid dynamics. *Biosyst. Eng., 103*(1), 78-99. https://doi.org/10.1016/j.biosystemseng.2009.02.007

Ogink, N. W., Mosquera, J., Calvet, S., & Zhang, G. (2013). Methods for measuring gas emissions from naturally ventilated livestock buildings: Developments over the last decade and perspectives for improvement. *Biosyst. Eng., 116*(3), 297-308. https://doi.org/10.1016/j.biosystemseng.2012.10.005

Özcan, S. E., Vranken, E., & Berckmans, D. (2009). Measuring ventilation rate through naturally ventilated air openings by introducing heat flux. *Build. Environ., 44*(1), 27-33. https://doi.org/10.1016/j.buildenv.2008.01.011

Saha, C. K., Ammon, C., Berg, W., Loebsin, C., Fiedler, M.,

Brunsch, R., & von Bobrutzki, K. (2013). The effect of external wind speed and direction on sampling point concentrations, air change rate, and emissions from a naturally ventilated dairy building. *Biosyst. Eng., 114*(3), 267-278. https://doi.org/10.1016/j.biosystemseng.2012.12.002

Samer, M., Loebsin, C., Fiedler, M., Ammon, C., Berg, W., Sanftleben, P., & Brunsch, R. (2011). Heat balance and tracer gas technique for airflow rates measurement and gaseous emissions quantification in naturally ventilated livestock buildings. *Energy Build., 43*(12), 3718-3728. https://doi.org/10.1016/j.enbuild.2011.10.008

Seifert, J., Li, Y., Axley, J., & Rosler, M. (2006). Calculation of wind-driven cross-ventilation in buildings with large openings. *J. Wind Eng. Ind. Aerodyn., 94*(12), 925-947. https://doi.org/10.1016/j.jweia.2006.04.002

Shilo, E., Teitel, M., Mahrer, Y., & Boulard, T. (2004). Airflow patterns and heat fluxes in roof-ventilated multi-span greenhouse with insect-proof screens. *Agric. Forest Meteorol., 122*(1), 3-20. https://doi.org/10.1016/j.agrformet.2003.09.007

Teitel, M., Liran, O., Tanny, J., & Barak, M. (2008a). Wind-driven ventilation of a mono-span greenhouse with a rose crop and continuous screened side vents and its effect on flow patterns and microclimate. *Biosyst. Eng., 101*(1), 111-122. https://doi.org/10.1016/j.biosystemseng.2008.05.012

Teitel, M., Tanny, J., Ben-Yakir, D., & Barak, M. (2005). Airflow patterns through roof openings of a naturally ventilated greenhouse and their effect on insect penetration. *Biosyst. Eng., 92*(3), 341-353. https://doi.org/10.1016/j.biosystemseng.2005.07.013

Teitel, M., Ziskind, G., Liran, O., Dubovsky, V., & Letan, R. (2008b). Effect of wind direction on greenhouse ventilation rate, airflow patterns, and temperature distributions. *Biosyst. Eng., 101*(3), 351-369. https://doi.org/10.1016/j.biosystemseng.2008.09.004

Van Buggenhout, S., Van Brecht, A., Eren Özcan, S., Vranken, E., Van Malcot, W., & Berckmans, D. (2009). Influence of sampling positions on accuracy of tracer gas measurements in ventilated spaces. *Biosyst. Eng., 104*(2), 216-223. https://doi.org/10.1016/j.biosystemseng.2009.04.018

Van Overbeke, P., De Vogeleer, G., Brusselman, E., Pieters, J. G., & Demeyer, P. (2015). Development of a reference method for airflow rate measurements through rectangular vents toward application in naturally ventilated animal houses: Part 3: Application in a test facility in the open. *Comput. Electron. Agric., 115*, 97-107. https://doi.org/10.1016/j.compag.2015.05.009

Van Overbeke, P., De Vogeleer, G., Pieters, J. G., & Demeyer, P. (2014b). Development of a reference method for airflow rate measurements through rectangular vents toward application in naturally ventilated animal houses: Part 2: Automated 3D approach. *Comput. Electron. Agric., 106*, 20-30. https://doi.org/10.1016/j.compag.2014.05.004

Van Overbeke, P., Pieters, J. G., De Vogeleer, G., & Demeyer, P. (2014a). Development of a reference method for airflow rate measurements through rectangular vents toward application in naturally ventilated animal houses: Part 1: Manual 2D approach. *Comput. Electron. Agric., 106*, 31-41. https://doi.org/10.1016/j.compag.2014.05.005

Wang, H., & Chen, Q. (2012). A new empirical model for predicting single-sided, wind-driven natural ventilation in buildings. *Energy Build., 54*, 386-394. https://doi.org/10.1016/j.enbuild.2012.07.028

Wang, S., Boulard, T., & Haxaire, R. (1999). Air speed profiles in a naturally ventilated greenhouse with a tomato crop. *Agric. Forest Meteorol., 96*(4), 181-188.

Wang, X., Ndegwa, P. M., Joo, H., Neerackal, G. M., Stockle, C. O., Liu, H., & Harrison, J. H. (2016). Indirect method versus direct method for measuring ventilation rates in naturally ventilated dairy houses. *Biosyst. Eng., 144*, 13-25. https://doi.org/10.1016/j.biosystemseng.2016.01.010

Wu, W., Zhai, J., Zhang, G., & Nielsen, P. V. (2012). Evaluation of methods for determining air exchange rate in a naturally ventilated dairy cattle building with large openings using computational fluid dynamics (CFD). *Atmos. Environ., 63*, 179-188. https://doi.org/10.1016/j.atmosenv.2012.09.042

Zhang, G., Strøm, J. S., Li, B., Rom, H. B., Morsing, S., Dahl, P., & Wang, C. (2005). Emission of ammonia and other contaminant gases from naturally ventilated dairy cattle buildings. *Biosyst. Eng., 92*(3), 355-364. https://doi.org/10.1016/j.biosystemseng.2005.08.002